Journal of Sound and Vibration (1999) **223**(3), 445–465
Article No. jsvi.1998.2097, available online at http://www.idealibrary.com on IDEAL®

EXACT SOLUTIONS FOR THE FREE AND FORCED VIBRATION OF A ROTATING DISK–SPINDLE SYSTEM

R. G. PARKER AND P. J. SATHE
Department of Mechanical Engineering, *The Ohio State University*, 206 *W*. 18*th Ave*., *Columbus*, *OH* 43201-1107, *U.S.A*.

(*Received* 10 *September* 1998, *and in final form* 23 *December* 1998)

Spinning disk–spindle systems consisting of an elastic disk mounted on an elastic spindle by means of a three-dimensional, rigid clamp extend the rich literature on spinning disks and spinning shafts that are decoupled from each other. This work presents an exact, closed-form solution for the eigensolutions of such systems. The complex eigenfunctions have the classical properties of a gyroscopic system when the individual disk, spindle and clamp deflections for a given eigenfunction are collected in terms of an extended eigenfunction. Eigenvalue perturbations are calculated to determine the sensitivity of the zero speed eigenvalues and the critical speeds to system parameters. Additionally, critical speeds analogous to those of a rigidly supported (classical) spinning disk are examined for the coupled system. Whereas the rigidly supported disk does not experience critical speed instability in the one-nodal diameter eigenfunctions, the coupled system does. The exact solution admits a closed-form modal analysis for the forced response to disk, spindle and clamp excitations. Response is calculated for two examples that demonstrate the strong disk–spindle modal coupling that can exist and the potentially damaging transmission of excitation energy between the disk and spindle.

1. INTRODUCTION

An extensive literature on the vibration and stability of spinning spindles (shafts) and spinning disks has been published in the last several decades. Much of the spinning shaft work has been motivated by power generation and transmission applications. Spinning disk analyses have been driven by circular saw, disk drive, disk brake, and similar systems. Analyses that model continuous system elastic vibration typically focus on either the spindle (with any attached disks modelled as rigid) or the disk (supported by a rigid structure). Practical systems such as disk drives, turbomachinery, and high-speed geared systems, however, exhibit *coupled* disk–spindle response wherein dynamic excitation at either the disk or spindle excites elastic vibration of both components. For example, the dominant excitation in gears is at the tooth mesh, but unacceptable noise is radiated primarily from the housing. The vibratory response is a coupled one involving

0022–460X/99/230445 + 21 $30.00/0

the disk, spindle, bearings, and housing. The reverse path occurs in disk drives where bearing forces and support structure motion drive disk vibration. While focusing on decoupled models, the existing literature also emphasizes free vibration and stability investigations with considerably less attention to operating condition response.

This study examines a *coupled* disk–spindle system where both the disk and spindle are elastic bodies; they are coupled by a rigid clamp (Figure 1). The associated eigenvalue problem is analytically solved in closed-form for the natural frequencies, vibration modes, and critical speeds. An examination of the critical speeds reveals that critical speeds associated with both the spindle and disk are present. These are analogous to the critical speeds of the individual, decoupled spindle and disk systems. Critical speeds analogous to those for a rigidly supported, spinning, elastic disk, termed *disk critical speeds* in this work, have not been previously discussed. The exact eigensolutions admit a

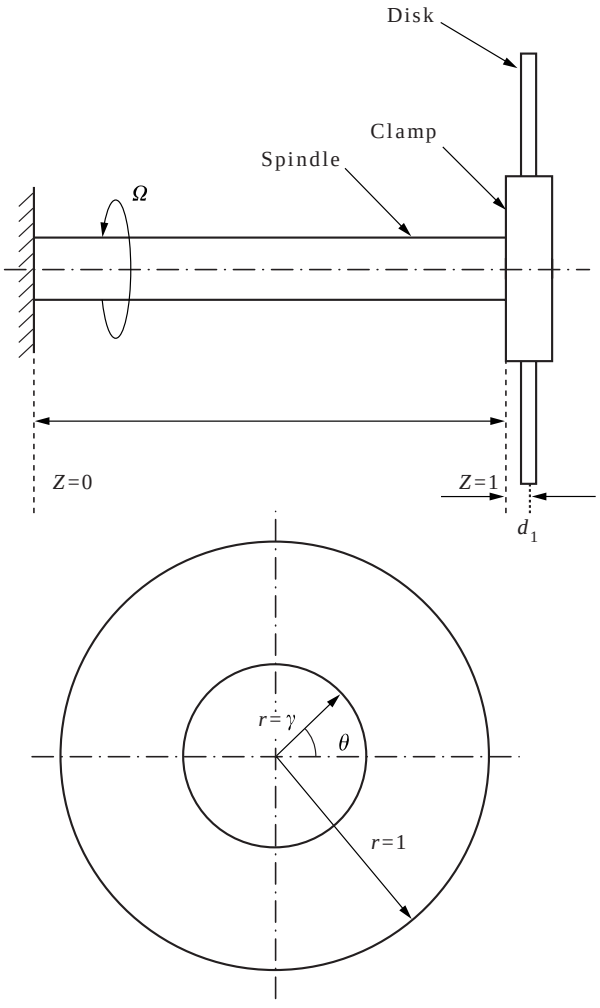

Figure 1. Disk–spindle system.

perturbation analysis for eigenvalue sensitivity and a gyroscopic system modal analysis to examine operating condition response. Response analyses for the cases of support motion and direct spindle excitation are presented to demonstrate the strongly coupled motions that can occur.

Flowers and Ryan [2] present a discussion of past literature [3–6] on coupled disk–spindle vibration, most of which is motivated by turbomachinery applications. This prior work generally uses transfer matrix methods and other lumped models to examine natural frequencies and critical speeds. None of these studies examine modal coupling and forced response. More recently, Lee *et al.* [7] numerically and experimentally studied the natural frequencies of a coupled disk–spindle system with application to disk drives. The present work builds on that of Chivens and Nelson [4], Parker [1], and Parker and Sathe [8]. Chivens and Nelson [4] analytically studied the natural frequencies of an elastic disk–spindle system coupled by a thin clamp. They conclude that disk flexibility alters the natural frequencies of an elastic spindle-*rigid* disk system but not the critical speeds. Parker [1] derived the linearized equations of motion for the system of Figure 1 with a three-dimensional clamp including certain practical asymmetries. He cast these in terms of extended operators that possess the standard symmetry and skew-symmetry properties of gyroscopic continua. This formulation admits classical analytical methods and is crucial for the perturbation and response analyses of the current work. Parker and Sathe [8] used the extended operator formulation to discretize the disk–spindle system using a Galerkin projection. They calculate natural frequencies over a broad range of parameters, identify the modal coupling that occurs in speed regions of natural frequency veering, and examine the character of the vibration modes. In contrast to the quantitative and qualitative characterization of the system eigensolutions conducted by Parker and Sathe [8], the present work presents few quantitative free vibration results but focuses instead on the derivation of the exact eigensolutions and the forced response. Discretization methods applied to gyroscopic systems may have poor accuracy or convergence at high speeds particularly when stationary system vibration modes are used as basis functions; the exact solution of this paper provides a valuable benchmark to confirm the accuracy of such approaches for both free and forced response.

2. EQUATIONS OF MOTION

Figure 1 shows the disk–spindle system in which an elastic, axisymmetric, rotating, cantilever spindle carries an elastic, axisymmetric disk at its end. A three-dimensional rigid clamp couples these components. The deformation is described by seven dimensionless variables: $w(r, \theta, t)$ is the transverse elastic deflection of the disk; $u(z, t)$ and $v(z, t)$ are the elastic deflections of the spindle in orthogonal planes; $u^c(t)$ and $v^c(t)$ are the displacements of the clamp center of mass; and $\phi(t)$ and $\psi(t)$ are the clamp rotations in the planes of the elastic deflections u and v, respectively. These seven variables are not independent because the clamp motions are related to the spindle deflections by the geometric compatibility conditions

$$\phi = u_z|_{z=1}, \quad \psi = v_z|_{z=1}, \quad u^c = u|_{z=1} + d_1\phi, \quad v^c = v|_{z=1} + d_1\psi. \tag{1}$$

The parameters of the system are

$$t = \bar{t}\sqrt{\frac{EI}{\rho_s l^4}}, \quad \Omega = \bar{\Omega}\sqrt{\frac{\rho_s l^4}{EI}}, \quad d_1 = \frac{\bar{d}_1}{l}, \quad K = \frac{D}{EI/l}, \quad \rho = \frac{\rho_d b^4}{\rho_s l^3}, \quad \alpha = \frac{m}{\rho_s l},$$

$$\gamma = \frac{a}{b}, \quad J_{ii}^{c,d} = \frac{\bar{J}_{ii}^{c,d}}{\rho_s l^5}, \quad q_d = \frac{\bar{q}_d}{EI/lb^3}, \quad q_{u,v} = \frac{\bar{q}_{u,v}}{EI/l^3}, \quad F_i = \frac{\bar{F}_i}{EI/l^2}, \quad M_i = \frac{\bar{M}_i}{EI/l}, \tag{2}$$

where $\bar{t}$ is the time, $\bar{\Omega}$ is the rotation speed, D is the disk flexural rigidity, EI is the spindle bending stiffness, ρ_d is the disk mass per unit area, ρ_s is the spindle mass per unit length, m is the combined mass of the clamp and the disk, a and b are the inner and outer radii of the disk, respectively, l is the length of the spindle, $\bar{d}_1$ is the clamp half-thickness (Figure 1), $\bar{J}_{ii}^c$ and $\bar{J}_{ii}^d$ are the moments of inertia of the clamp and the disk, $\bar{q}_d$ is the transverse disk force, $\bar{q}_u$ and $\bar{q}_v$ are the transverse spindle forces, and $\bar{F}_i$ and $\bar{M}_i$ are the applied forces and moments on the clamp. Parker [1] derived the linearized equations of motion of the system in rotating co-ordinates including several asymmetries. The dimensionless equations for the *axisymmetric* system are

$$K\nabla^4 w - \Omega^2\xi(w) + \rho[w_{tt} - r\cos\theta(\phi_{tt} + \Omega^2\phi) - r\sin\theta(\psi_{tt} + \Omega^2\psi)] = q_d(r, \theta, t), \tag{3}$$

$$u_{zzzz} + u_{tt} - 2\Omega v_t - \Omega^2 u = q_u(z, t), \tag{4}$$

$$v_{zzzz} + v_{tt} + 2\Omega u_t - \Omega^2 v = q_v(z, t), \tag{5}$$

$$-u_{zzz}|_{z=1} + \alpha u_{tt}^c - 2\Omega\alpha v_t^c - \Omega^2\alpha u^c = F_1(t), \tag{6}$$

$$-v_{zzz}|_{z=1} + \alpha v_{tt}^c + 2\Omega\alpha u_t^c - \Omega^2\alpha v^c = F_2(t), \tag{7}$$

$$u_{zz}|_{z=1} + d_1 u_{zzz}|_{z=1} + (J_{22}^c + J_{22}^d)\phi_{tt} - \int\int \rho r\cos\theta w_{tt}\, \mathrm{d}A$$
$$- \Omega(J_{11}^c + J_{22}^c - J_{33}^c)\psi_t - \Omega^2\left[(J_{11}^c - J_{33}^c - J_{22}^d)\phi + \int\int \rho r\cos\theta w\, \mathrm{d}A\right] = M_2(t), \tag{8}$$

$$v_{zz}|_{z=1} + d_1 v_{zzz}|_{z=1} + (J_{11}^c + J_{11}^d)\psi_{tt} - \int\int \rho r \sin\theta w_{tt}\, \mathrm{d}A$$
$$+ \Omega(J_{11}^c + J_{22}^c - J_{33}^c)\phi_t - \Omega^2\left[(J_{22}^c - J_{33}^c - J_{11}^d)\psi + \int\int \rho r \sin\theta w\, \mathrm{d}A\right] = -M_1(t). \tag{9}$$

Here, r and θ are polar co-ordinates in a frame fixed to the rotating disk, and z is the co-ordinate of a material point on the spindle. Equations (3)–(5) are the governing equations over the continuous disk and spindle domains, equations (6) and (7) are the linear momentum balances for the clamp, and equations (8) and (9) are the angular momentum balances for the clamp. $\xi(w)$ is the membrane stress operator [9]:

$$\Omega^2\xi(w) = \frac{1}{r}(r\sigma^r w_r)_r + \frac{1}{r}\left(\frac{1}{r}\sigma^\theta w_\theta\right)_\theta, \tag{10}$$

$$\sigma^r = \Omega^2\left(c_1 + \frac{c_2}{r^2} + c_3 r^2\right), \quad \sigma^\theta = \Omega^2\left(c_1 - \frac{c_2}{r^2} + c_4 r^2\right), \tag{11}$$

$$c_1 = \rho\left(\frac{1+\nu}{8}\right)\frac{(\nu-1)\gamma^4 - (3+\nu)}{(\nu-1)\gamma^2 - (1+\nu)}, \quad c_2 = \rho\frac{1-\nu}{8}\nu^2\frac{(\nu+1)\gamma^2 - (3+\nu)}{(\nu-1)\gamma^2 - (1+\nu)},$$
$$c_3 = -\rho\frac{3+\nu}{8}, \quad c_4 = -\rho\frac{1+3\nu}{8}; \tag{12}$$

$\sigma^{r,\theta}$ are the disk rotational stresses and ν is Poisson's ratio. The spindle and disk boundary conditions are

$$u|_{z=0} = v|_{z=0} = 0, \quad u_z|_{z=0} = v_z|_{z=0} = 0,$$
$$w|_{r=\gamma} = 0, \quad \left[\nabla^2 w - \frac{1-\nu}{r}\left(w_r + \frac{w_{\theta\theta}}{r}\right)\right]_{r=1} = 0,$$
$$w_r|_{r=\gamma} = 0, \quad \left[(\nabla^2 w)_r - \frac{1-\nu}{r^2}\left(\frac{w_{\theta\theta}}{r} - w_{r\theta\theta}\right)\right]_{r=1} = 0. \tag{13}$$

Equations (3)–(9) can be written in a structured manner using the extended operator formulation [1, 10]. Defining the extended variable $\mathbf{h}$ as

$$\mathbf{h}(r, \theta, z, t) = [w(r, \theta, t)\ u(z, t)\ v(z, t)\ u^c(t)\ v^c(t)\ \phi(t)\ \psi(t)]^T, \tag{14}$$

equations (3)–(9) are written concisely as

$$\mathbf{M}\mathbf{h}_{tt} + \Omega\mathbf{G}\mathbf{h}_t + (\mathbf{L} - \Omega^2\tilde{\mathbf{L}})\mathbf{h} = \mathbf{f}, \tag{15}$$

where $\mathbf{M}$, $\mathbf{G}$, $\mathbf{L}$, and $\tilde{\mathbf{L}}$ are the extended operators operating on $\mathbf{h}$ and $\mathbf{f}$ is the extended excitation vector. These operators are defined in Parker [1]. The inner

product between two extended variables $\mathbf{x}$ and $\mathbf{y}$ is defined as

$$(\mathbf{x}, \mathbf{y}) = \int\int x_1\bar{y}_1 \, \mathrm{d}A + \int_0^1 x_2\bar{y}_2 \, \mathrm{d}z + \int_0^1 x_3\bar{y}_3 \, \mathrm{d}z + x_4\bar{y}_4 + x_5\bar{y}_5 + x_6\bar{y}_6 + x_7\bar{y}_7, \quad (16)$$

where x_i and y_i are the elements of the extended variables $\mathbf{x}$ and $\mathbf{y}$, the double integral is over the area of the disk, the single integrals are over the length of the spindle, and the overbar denotes complex conjugate. With this inner product and the constraints (1), the operators $\mathbf{M}$, $\mathbf{L}$ and $\tilde{\mathbf{L}}$ are symmetric and $\mathbf{G}$ is skew-symmetric. Moreover, $\mathbf{M}$ and $\mathbf{L}$ are positive definite. Thus, equations (15) and (16) cast the disk–spindle system in the canonical form of a gyroscopic continuum. The importance of this structured formulation will be evident in the perturbation analysis and the forced response discussed later.

3. EXACT SOLUTION OF THE EIGENVALUE PROBLEM

An exact analytical solution of the gyroscopic system eigenvalue problem is presented here. Use of the separable solutions $u(z, t) = \zeta(z)\mathrm{e}^{\lambda t}$ and $v(z, t) = \eta(z)\mathrm{e}^{\lambda t}$ in the spindle equations (4) and (5) gives

$$\zeta_{zzzz} + \lambda^2\zeta - 2\Omega\lambda\eta - \Omega^2\zeta = 0, \quad \eta_{zzzz} + \lambda^2\eta + 2\Omega\lambda\zeta - \Omega^2\eta = 0. \quad (17, 18)$$

Decoupling these equations yields

$$\frac{\mathrm{d}^8\zeta}{\mathrm{d}z^8} + 2(\lambda^2 - \Omega^2)\frac{\mathrm{d}^4\zeta}{\mathrm{d}z^4} + (\lambda^2 + \Omega^2)^2\zeta = 0 \quad (19)$$

and an identical equation for η. The general solution of equation (19) is

$$\begin{aligned}\zeta(z) = {} & A_1\cos\alpha z + A_2\sin\alpha z + A_3\cosh\alpha z + A_4\sinh\alpha z \\ & + A_5\cos\beta z + A_6\sin\beta z + A_7\cosh\beta z + A_8\sinh\beta z, \end{aligned} \quad (20)$$

where A_i are complex constants, $\alpha = (-\lambda^2 + \Omega^2 + 2i\lambda\Omega)^{1/4}$ and $\beta = (-\lambda^2 + \Omega^2 - 2i\lambda\Omega)^{1/4}$. The solution for $\eta(z)$ is identical to equation (20) with C_i replacing A_i. Substitution of the $\eta(z)$ solution and equation (20) into equation (17) (or equation (18)) yields

$$\begin{aligned}\eta(z) = {} & -iA_1\cos\alpha z - iA_2\sin\alpha z - iA_3\cosh\alpha z - iA_4\sinh\alpha z \\ & + iA_5\cos\beta z + iA_6\sin\beta z + iA_7\cosh\beta z + iA_8\sinh\beta z. \end{aligned} \quad (21)$$

The eigenfunctions are complex as seen in equations (20) and (21).

The separable solution $w(r, \theta, t) = w(r, \theta)\mathrm{e}^{\lambda t}$ reduces equation (3) to

$$K\nabla^4 w - \Omega^2\xi + \rho[\lambda^2(w - r\cos\theta\phi - r\sin\theta\psi) - \Omega^2(r\cos\theta\phi \; r\sin\theta\psi)] = 0. \quad (22)$$

For an axisymmetric disk, disk–spindle couplng occurs only for the one-nodal diameter eigenfunctions [3, 10]. These are the *coupled* modes of the system and the only ones of interest here. For numbers of nodal diameters other than one, the deformation is only in the disk; the spindle does not deform. These are the *uncoupled* modes of the system; they are well known from analyses of rigidly

supported disks. For the coupled modes, the solution

$$w(r, \theta) = g(r)\cos\theta + p(r)\sin\theta \tag{23}$$

gives the radial part of the disk equation from equation (22),

$$\begin{aligned} r^4\frac{\mathrm{d}^4 g}{\mathrm{d}r^4} + 2r^3\frac{\mathrm{d}^3 g}{\mathrm{d}r^3} - [3r^2 + \delta^2(c_1 r^4 + c_2 r^2 + c_3 r^6)]\frac{\mathrm{d}^2 g}{\mathrm{d}r^2} \\ + [3r - \delta^2(c_1 r^3 - c_2 r + c_4 r^5 - \rho r^5)]\frac{\mathrm{d}g}{\mathrm{d}r} \\ - \left[3 - \delta^2(c_1 r^2 - c_2 + c_4 r^4) + r^4\omega^2\left(\frac{\rho}{K}\right)\right]g \\ = \delta^2\rho r^5\phi - \omega^2\left(\frac{\rho}{K}\right)r^5\phi, \end{aligned} \tag{24}$$

where $\delta = \Omega/\sqrt{K}$ and $\lambda = i\omega$. An identical equation is obtained for $p(r)$ with ϕ replaced by ψ. The solution of equation (24) is obtained using the power series method [11]. Using an expansion about the ordinary point $r = 1$, the homogeneous solution has the form

$$g(r) = \sum_{n=0}^{\infty} a_n (1 - r)^n. \tag{25}$$

Substituting this in the homogeneous form of equation (24) and equating coefficients of each power of $(1 - r)$ to zero, it is found that the coefficients a_0–a_3 are arbitrary, a_4–a_7 depend on a_0–a_3, and each of the higher coefficients depends on the previous eight coefficients. The recursion relation for $n \geqslant 4$ is

$$\begin{aligned} a_{n+4} = -\{&-[4(n+3)(n+2)(n+1)n + 2(n+3)(n+2)(n+1)]a_{n+3} \\ &+ [6(n+2)(n+1)n(n-1) + 6(n+2)(n+1)n \\ &+ (-3 - \delta^2(c_1 + c_2 + c_3))(n+2)(n+1)]a_{n+2} \\ &+ [-4(n+1)n(n-1)(n-2) - 6(n+1)n(n-1) \\ &+ (6 - \delta^2(-4c_1 - 2c_2 - 6c_3))(n+1)n \\ &- (3 - \delta^2(c_1 - c_2 + c_4 - \rho))(n+1)]a_{n+1} + [n(n-1)(n-2)(n-3) \\ &+ 2n(n-1)(n-2) + (-3 - \delta^2(6c_1 + c_2 + 15c_3))n(n-1) \\ &+ (3 + \delta^2(-3c_1 + c_2 - 5c_4 + 5\rho))n + (-3 + \delta^2(c_1 - c_2 + c_4) - \omega^2\rho/K)]a_n \\ &+ [-\delta^2(-4c_1 - 20c_3)(n-1)(n-2) + \delta^2(3c_1 + 10c_4 - 10\rho)(n-1) \\ &+ \delta^2(-2c_1 - 4c_4) + 4\omega^2\rho/K]a_{n-1} \end{aligned}$$

$$+ [-\delta^2(c_1 + 15c_3)(n-2)(n-3)$$
$$+ \delta^2(-c_1 - 10c_4 + 10\rho)(n-2) + \delta^2(c_1 + 6c_4) - 6\omega^2\rho/K]a_{n-2}$$
$$+ [6\delta^2 c_3(n-3)(n-4) + \delta^2(5c_4 - 5\rho)(n-3) + (-4\delta^2 c_4 + 4\omega^2\rho/K)]a_{n-3}$$
$$+ [-\delta^2 c_3(n-4)(n-5) + \delta^2(-c_4 + \rho)(n-4)$$
$$+ \delta^2 c_4 - \omega^2\rho/K]a_{n-4}\}/\{(n+4)(n+3)(n+2)(n+1)\}. \tag{26}$$

Substitution of $n = 0$ in the recursion relation and setting the coefficients with negative subscripts to zero gives the expression for a_4 in terms of a_0–a_3. Similarly, substituting $n = 1$ and the expression for a_4 into the recursion relation gives a_5 in terms of a_0–a_3. This procedure is repeated to obtain a_4–a_7 in terms of a_0–a_3. Finally, setting one of the coefficients a_0–a_3 equal to one and the other three equal to zero at a time in the power series (25) gives four independent homogeneous solutions w_{0h_1}–w_{0h_4} of equation (24). The general solution (23) to the disk equation is

$$w(r, \theta) = (B_1 w_{0h_1} + B_2 w_{0h_2} + B_3 w_{0h_3} + B_4 w_{0h_4} + r\phi)\cos\theta$$
$$+ (B_5 w_{0h_1} + B_6 w_{0h_2} + B_7 w_{0h_3} + B_8 w_{0h_4} + r\psi)\sin\theta, \tag{27}$$

where $r\phi$ is a particular solution of equation (24), B_i are complex constants, and the $p(r)\sin\theta$ term of equation (23) has been included.

Insertion of equations (20), (21) and (27) into equations (6)–(9), (13), and (1) yields 16 linear, homogeneous equations in the 16 coefficients A_i and B_i. Roots of the characteristic determinant give the natural frequencies ω.

The disk and spindle modal deflections (27), (20) and (21) are collected into an extended eigenfunction of the form (14) where the modal deflections and rotations of the clamp are calculated from equation (1):

$$\mathbf{h}_m = \begin{pmatrix} w_m = g_m(r)\cos\theta + p_m(r)\sin\theta \\ \zeta_m(z) \\ \eta_m(z) \\ u_m^c = \zeta_m(1) + d_1\zeta_{m_z}(1) \\ v_m^c = \eta_m(1) + d_1\eta_{m_z}(1) \\ \phi = \zeta_{m_z}(1) \\ \psi = \eta_{m_z}(1) \end{pmatrix}, \quad m = 1, 2, \ldots. \tag{28}$$

Note that equation (28) is the form for the complex *coupled* modes. They occur in complex conjugate pairs. The *uncoupled* modes, which are real and degenerate, have the form

$$\mathbf{h}_n = [R_n(r)(a_1\cos n\theta + a_2\sin n\theta)\ 0\ 0\ 0\ 0\ 0\ 0]^{\mathrm{T}}, \quad n \neq 1, \tag{29}$$

where a_1 and a_2 are arbitrary constants. The coupled vibration modes are qualitatively classified as *disk modes*, in which the strain energy in the disk

dominates the total strain energy, and *spindle modes*, in which the strain energy in the spindle dominates the total modal strain energy [8].

The above solution can be specialized to solve two special cases: the zero speed eigenvalue problem ($\Omega = 0$), and the critical speed eigenvalue problem to determine the speeds at which an eigenvalue vanishes ($\omega = 0$). To distinguish from *disk critical speeds* introduced later, the term *spindle critical speeds* is used for speeds with vanishing eigenvalues as these critical speeds exist for a spindle not coupled to a disk. At such spindle critical speeds, static loads in the rotating frame (e.g., a center of mass offset from the rotation axis) excite a resonance condition. The recursion relations for these problems are obtained by substituting $\Omega = 0$ or $\omega = 0$ into equation (26). Homogeneous solutions of the disk equation for the zero speed eigenvalue problem are Bessel functions. For both $\Omega = 0$ and $\omega = 0$, the following simplifications occur: equations (4) and (5) reduce to decoupled stationary beam equations with well-known solutions, the spindle deforms in only one plane for each mode, and the order of the characteristic determinant is 8 as opposed to 16 because of this decoupling. All roots (that is, zero speed natural frequencies and spindle critical speeds) of the characteristic determinant are degenerate and the two associated modes are identical except for the plane of motion.

The choice of the point of expansion for the power series (25) varies in the literature. Lamb and Southwell [12] used the regular singular point $r = 0$, whereas Eversman and Dodson [13] and Chivens and Nelson [4] used the ordinary point $r = 1$. In order to check whether expansion about one point leads to better convergence than the other, an approach identical to that above was used to obtain the natural frequencies by expanding about $r = 0$, that is

$$g(r) = \sum_{n=0}^{\infty} a_n r^{n+\alpha}$$

This method, however, gave only the first two natural frequencies at each speed, as shown in Table 2, irrespective of the number of terms retained in the power series. Moreover, the convergence for $r = 0$ is slower than that for $r = 1$. The choice $r = 1$ is superior to $r = 0$ for the parameter set considered here, and an expansion about $r = 1$ is used in the subsequent results.

The exact solution provides a valuable benchmark for evaluation of approximate methods. The comparison between the exact solution and the Galerkin solution in Parker and Sathe [8] is shown in Figure 2. Only the natural

TABLE 1

Non-dimensional parameters for the disk–spindle system

$K = 0{\cdot}000355$	$\rho = 0{\cdot}022279$
$d_1 = 0{\cdot}032480$	$\alpha = 2{\cdot}05774$
$\gamma = 0{\cdot}5$	$J^c_{11} = 0{\cdot}029521$
$J^c_{22} = 0{\cdot}029521$	$J^c_{33} = 0{\cdot}057743$
$J^d_{11} = 0{\cdot}016404$	$J^d_{22} = 0{\cdot}016404$
$J^d_{33} = 0{\cdot}032808$	$\nu = 0{\cdot}28$

TABLE 2

Convergence of the lowest three dimensionless natural frequencies for power series expansion about $r = 0$ and $r = 1$ for $\Omega = 0{\cdot}5$, 1 and 2. Parameters used are given in Table 1

		$r = 0$ Number of terms				$r = 1$ Number of terms		
Ω	Galerkin	20	40	60	80	20	40	60
	0·593	0·593	0·593	0·593	0·593	0·593	0·593	0·593
0·5	1·528	1·558	1·555	1·554	1·552	1·528	1·528	1·528
	1·844					1·844	1·844	1·844
	0·113	0·114	0·113	0·113	0·113	0·113	0·113	0·113
1	1·987	2·036	2·032	2·031	2·030	1·988	1·987	1·987
	2·267					2·268	2·267	2·267
	0·852	0·870	0·852	0·852	0·852	0·852	0·852	0·852
2	2·948	2·979	2·977	2·976	2·974	2·950	2·948	2·948
	3·457					3·458	3·457	3·457

frequencies of the coupled one-nodal diameter modes are shown. Excellent agreement with the exact solution is observed for all eigenvalues even for extremely high speeds. The Galerkin solution employed 12 zero speed eigenfunctions (six degenerate pairs) as basis functions at each speed. The exact

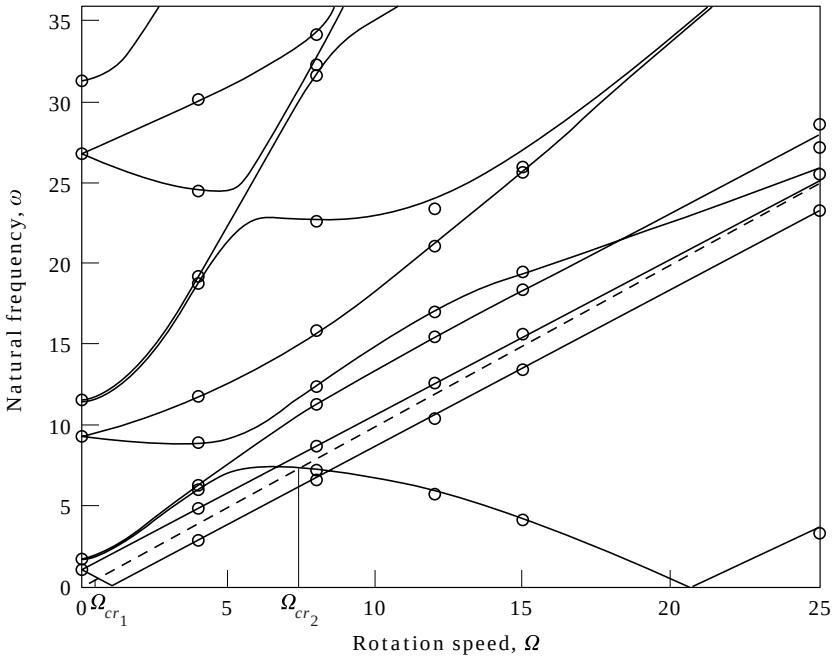

Figure 2. Comparison between exact natural frequencies (denoted by circles) and Galerkin [8] natural frequencies (solid curves) for a rotating disk–spindle system. Parameters are given in Table 1. The dashed line has unity slope. Its points of intersection with the solid lines are the *disk* critical speeds Ω_{cr_i}.

solution requires 40 terms to converge at $\Omega = 2$, as shown in Table 2; more terms are necessary at higher speeds. Validation of the Galerkin results is important as Galerkin discretization is far more convenient than the exact solution from the perspectives of programming ease and computational efficiency. The accuracy of the Galerkin discretization cannot be taken for granted in the absence of a verifying exact solution, however, as discretization methods for gyroscopic systems at high speeds may converge poorly and yield erroneous results [14, 15]. An advantage of the Galerkin solution is that the inertia, gyroscopic, and stiffness matrices are independent of speed and are calculated only once.

A key feature of the above complex, speed-dependent eigenfunctions is that they likely provide an excellent basis for discretization of models with non-linear, time-varying, and dissipative effects that are present in practical systems. For example, axially moving media systems (which are gyroscopic systems) demonstrate excellent convergence when complex, speed-dependent eigenfunctions are used in the discretization [14]. Similar behavior can be expected for other gyroscopic continua because the basis functions adapt to the changing speed. The difficulty, however, is in analytically calculating the speed-dependent eigenfunctions of a simpler, related gyroscopic system. The complex, speed-dependent eigenfunctions herein provide the necessary basis functions for spinning disk–spindle systems, and one would expect more rapid convergence compared to the stationary system eigenfunctions or other speed-independent basis functions.

4. DISK CRITICAL SPEEDS

The spindle critical speeds at which an eigenvalue vanishes in Figure 2 are only part of the complete critical speed picture. In addition to these critical speeds derived from the gyroscopic terms in the spindle equations of motion, there are also *disk critical speeds* where the name reflects the association with the critical speeds of a classical spinning disk. To understand this concept, first consider the critical speeds of a classical, rigidly supported disk.

The critical speeds of a rigidly supported, spinning disk are the speeds at which a disk natural frequency in a ground-based (inertial) reference frame is zero [16]. At such speeds any constant, stationary force applied to the disk leads to large amplitude resonant response. In a rotating reference frame, the critical speeds are given by $\Omega_{cr} = \omega_n/n$ where ω_n is the natural frequency in the rotating reference frame and $n \neq 0$ is the number of nodal diameters in the associated mode. To see the relationship between the fixed and rotating frame characterizations, consider a stationary point force of unit magnitude acting on the disk perpendicular to its plane. In the rotating frame, the excitation appears as the rotating force $F_d = \delta(r - r_0)\delta(\theta + \Omega t)/r_0$ where $\delta(\cdot)$ is the Dirac delta function. The modal force associated with the n-nodal diameter mode $w_n(r, \theta) = R_n(r) \cos n\theta$ is

$$f_n = \int\int F_d(r, \theta, t) w_n(r, \theta)\, \mathrm{d}A = R_n(r_0) \cos n\Omega t. \tag{30}$$

Resonant response (i.e., a critical speed) occurs when $n\Omega = \omega_n$ as noted previously. One would expect modes having any number of nodal diameters other than zero to become critical at some speed, but Renshaw and Mote [17] proved that the one-nodal diameter modes of a rigidly supported disk never become critical. These modes, however, do become critical for the coupled disk–spindle system as discussed below.

We use the stationary force interpretation to characterize the disk critical speeds of the coupled system. The extended excitation vector $\mathbf{f}$ associated with a stationary point force on the disk is $\mathbf{f} = [F_d\ 0\ 0\ 0\ 0\ 0\ 0]^T$ where F_d is as given above. The modal force associated with the *uncoupled* extended eigenfunctions $\mathbf{h}_n$ of equation (29) (with $a_1 = 1$ and $a_2 = 0$) is

$$f_n = (\mathbf{h}_n, \mathbf{f}) = R_n(r_0)\cos n\Omega t, \quad n \neq 1, \tag{31}$$

which is identical to equation (30). Resonant response occurs when $n\Omega = \omega_n$ $(n \neq 1)$, as for the rigidly supported disk. Because the *uncoupled* vibration modes $(n \neq 1)$ and corresponding rotating frame natural frequencies ω_n of a disk–spindle system are exactly those of a rigidly supported disk [1], the disk critical speeds of the uncoupled modes are unaffected by disk–spindle coupling. Thus, the coupled system is subject to the same critical speed instabilities as the rigidly supported disk; the unstable critical modes are identical to those of a rigidly supported disk and involve purely disk deformation.

Considering now the coupled vibration modes $\mathbf{h}_m$ of equation (28), the associated modal force is

$$f_m = (\mathbf{h}_m, \mathbf{f}) = g_m(r_0)\cos\Omega t - p_m(r_0)\sin\Omega t, \quad m = 1, 2, \ldots. \tag{32}$$

Resonance occurs for $\Omega = \omega_m$, where ω_m are the coupled, one-nodal diameter natural frequencies, and this condition defines the disk critical speeds corresponding to the coupled modes. This condition is satisfied as is evident from Figure 2, where the lowest disk critical speed is actually lower than the lowest spindle critical speed ($\omega = 0$). Thus, in contrast to the rigidly supported disk, critical speed instabilities of the one-nodal diameter modes, which are the coupled modes of the disk–spindle system, *do* occur. The severity of a disk critical speed instability depends on whether the critical coupled mode involves predominantly disk or spindle deformation. For the parameter set considered in Table 1, the critical modes at all disk critical speeds are predominantly spindle modes. For these modes the modal force given by equation (32) is small. As a result, the instability may not be severe in light of the small damping inherently present in the system that limits the resonant response amplitude. A more dangerous situation exists when the critical coupled mode is predominantly a disk mode, as the resonant response induced by stationary disk forces would be driven by a larger modal force.

In summary, spindle critical speeds exist at zero eigenvalues of the coupled system as viewed in the rotating frame. The critical modes are all coupled modes as pure spindle modes do not exist. Disk critical speeds exist for the uncoupled modes (pure disk deformation) at exactly the same critical speeds as for the rigidly supported disk, that is, $\Omega_{cr} = \omega_n/n$, where ω_n are the rotating frame

natural frequencies of the uncoupled modes (not shown in Figure 2). Disk critical speeds exist for the coupled modes when $\Omega = \omega_m$, where ω_m are the natural frequencies of the coupled modes as given in Figure 2.

5. NATURAL FREQUENCY SENSITIVITY TO SYSTEM PARAMETERS

The extended operator structure allows application of eigenvalue perturbation to examine the sensitivity of the natural frequencies and critical speeds to the non-dimensional parameters. To demonstrate the approach, consider perturbation of the disk–spindle stiffness ratio, $K = K_0 + \varepsilon K'$. Defining $\mathbf{L}'\mathbf{a}_0 = [K'\nabla^4\omega_0\ 0\ 0\ 0\ 0\ 0\ 0]^{\mathrm{T}}$, the zero speed eigenvalue problem in terms of extended operators is

$$(\mathbf{L} + \varepsilon\mathbf{L}')\mathbf{a} - \omega^2\mathbf{M}\mathbf{a} = \mathbf{0}, \tag{33}$$

with appropriate homogeneous boundary conditions. Here, $\mathbf{a}$ is the extended eigenfunction associated with the natural frequency ω, where $\lambda = i\omega$ is the eigenvalue. ω and $\mathbf{a}$ are represented as

$$\omega^2 = \omega_0^2 + \varepsilon\mu, \quad \mathbf{a} = \mathbf{a}_0 + \varepsilon\mathbf{a}_1. \tag{34}$$

Substitution of equation (34) into equation (33) leads to

$$\mathbf{L}\mathbf{a}_0 - \omega_0^2\mathbf{M}\mathbf{a}_0 = \mathbf{0}, \tag{35}$$

$$\mathbf{L}\mathbf{a}_1 - \omega_0^2\mathbf{M}\mathbf{a}_1 = -\mathbf{L}'\mathbf{a}_0 + \mu\mathbf{M}\mathbf{a}_0, \tag{36}$$

where the appropriate boundary conditions are appended to equations (35) and (36). The unperturbed eigenvalue problem (35) can be solved analytically [10]. Each of its natural frequencies is degenerate, so $\mathbf{a}_0 = d_1\mathbf{a}_{01} + d_2\mathbf{a}_{02}$, where $\mathbf{a}_{01}$ and $\mathbf{a}_{02}$ are the unperturbed eigenfunctions associated with ω_0, and d_1 and d_2 are constants to be determined. The $\mathbf{a}_{0i}$ satisfy the orthonormality conditions $(\mathbf{a}_{0i}, \mathbf{M}\mathbf{a}_{0i}) = \delta_{ij}$. Solvability conditions from equation (36) yield

$$\mu d_1 = d_1(\mathbf{a}_{01}, \mathbf{L}'\mathbf{a}_{01}), \quad \mu d_2 = d_2(\mathbf{a}_{02}, \mathbf{L}'\mathbf{a}_{02}). \tag{37}$$

Expansion of equation (37) yields the equivalent conditions

$$\mu = K' \int\int (w_0 \cos\theta)\nabla^4(w_0 \cos\theta)\ \mathrm{d}A = K' \int\int (w_0 \sin\theta)\nabla^4(w_0 \sin\theta)\ \mathrm{d}A, \tag{38}$$

where $w_0(r)$ is the radial component of the disk deflection for $\mathbf{a}_{01}$ and $\mathbf{a}_{02}$. The biharmonic operator is positive definite, so μ is positive and the zero speed natural frequencies increase with K (Figure 3).

The spindle critical speed eigenvalue problem is

$$(\mathbf{L} + \varepsilon\mathbf{L}')\mathbf{b} - \Omega_{cr}^2\tilde{\mathbf{L}}\mathbf{b} = \mathbf{0}, \tag{39}$$

with homogeneous boundary conditions. $\mathbf{b}$ is the extended critical speed eigenfunction. With the representations $\mathbf{b} = \mathbf{b}_0 + \varepsilon\mathbf{b}_1$, $\Omega_{cr}^2 = \Omega_{cr_0}^2 + \varepsilon\delta$,

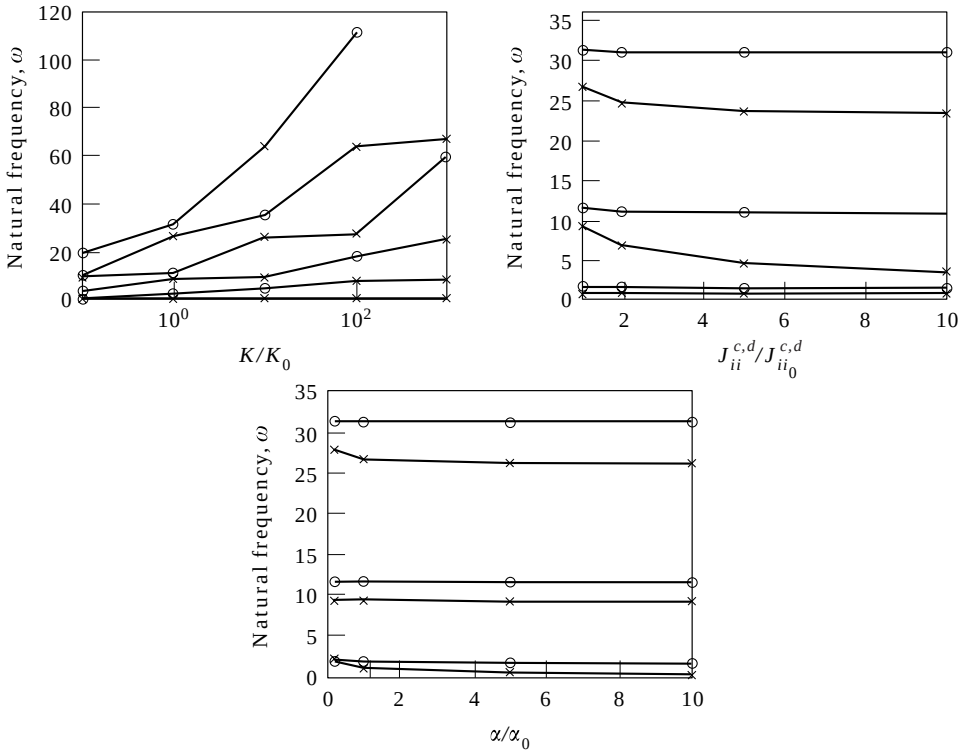

Figure 3. Variation of the zero speed natural frequencies with the non-dimensional parameters K, $J_{ii}^{c,d}$ and α. The parameters K_0, $J_{ii_0}^{c,d}$ and α_0 are as in Table 1. The circles denote disk natural frequencies and the crosses denote spindle natural frequencies.

perturbation yields

$$\delta = \frac{K' \int\int (w_{cr}\cos\theta)\nabla^4(w_{cr}\cos\theta)\,\mathrm{d}A}{(\mathbf{b}_{01}, \tilde{\mathbf{L}}\mathbf{b}_{01})} = \frac{K' \int\int (w_{cr}\sin\theta)\nabla^4(w_{cr}\sin\theta)\,\mathrm{d}A}{(\mathbf{b}_{02}, \tilde{\mathbf{L}}\mathbf{b}_{02})}, \quad (40)$$

where $\mathbf{b}_{01}$ and $\mathbf{b}_{02}$ are the degenerate critical speed eigenfunctions and $w_{cr}(r)$ is the radial component of the disk deflection for $\mathbf{b}_{01}$ and $\mathbf{b}_{02}$. Consider the unperturbed critical speed eigenvalue problem $\mathbf{L}\mathbf{b}_{0i} - \Omega_{cr_0}^2 \tilde{\mathbf{L}}\mathbf{b}_{0i} = \mathbf{0}$. The associated Rayleigh Quotient is $\Omega_{cr_0}^2 = (\mathbf{b}_{0i}, \mathbf{L}\mathbf{b}_{0i})/(\mathbf{b}_{0i}, \tilde{\mathbf{L}}\mathbf{b}_{0i})$. Because $\Omega_{cr_0}^2$ is positive and $\mathbf{L}$ is positive definite, the inner product $(\mathbf{b}_{0i}, \tilde{\mathbf{L}}\mathbf{b}_{0i})$ is positive for critical speed eigenfunctions $\mathbf{b}_{0i}$. Thus, $\delta > 0$ and the spindle critical speeds increase with K.

Analogous results when all elements of the inertia tensors are perturbed simultaneously, that is $J_{ii}^{c,d} = J_{ii_0}^{c,d} + \varepsilon J_{ii}^{c,d'}$, are

$$\mu = -(J_{22}^{c'} + J_{22}^{d'})\omega_0^2\phi_0^2 < 0, \quad \delta = \frac{(J_{33}^{c'} + J_{22}^{d'} - J_{11}^{c'})\Omega_{cr}^2\phi_{cr}^2}{(\mathbf{b}_{0i}, \tilde{\mathbf{L}}\mathbf{b}_{0i})}. \quad (41)$$

Perturbation of the clamp mass parameter α according to $\alpha = \alpha_0 + \varepsilon\alpha'$ yields the zero speed natural frequency and spindle critical speed perturbations

TABLE 3

Perturbations for the critical speed eigenvalue problem. The perturbations K', $J_{ii}^{cd\prime}$ and α' are assigned values 10% of the corresponding values in Table 1 and the critical speed perturbations δ_i are calculated. The table shows the ratios of δ_i to $\Omega_{cr_i}^2$

Parameter	Critical speed perturbation (%) $\frac{\delta_1}{\Omega_{cr_1}^2}$	$\frac{\delta_2}{\Omega_{cr_2}^2}$
K	5·65e-4	1·733e-6
$J_{ii}^{c,d}$	0·204	0·067
α	−4·68	−0·418

$$\mu = -\alpha' \omega_0^2 u_0^{c2} < 0, \quad \delta = \frac{-\alpha' \Omega_{cr}^2 u_{cr}^{c2}}{(\mathbf{b}_{0i}, \tilde{\mathbf{L}}\mathbf{b}_{0i})} < 0. \tag{42}$$

Figure 3 shows the natural frequencies obtained by solving the stationary system eigenvalue problem for different values of the non-dimensional parameters considered above. The calculated results are consistent with the perturbation predictions. Table 3 shows δ_i as a percentage of Ω_{cri}^2 when the perturbations K', $J_{ii}^{c,d'}$ and α' are assigned values 10% of the corresponding values in Table 1. While the dimensionless spindle critical speeds follow the trends predicted by the perturbation analysis, their changes are small. In fact, spindle critical speed curves analogous to those in Figure 3 remain virtually flat across the same parameter ranges as Figure 3.

6. FORCED RESPONSE

An important feature of the analytical eigensolution for the rotating system is that, in conjunction with the extended operators, it admits a gyroscopic system modal analysis [18, 19] to obtain the response to external excitation. Parker [1] applied this procedure to obtain formal expressions for the rotating disk–spindle response using the extended operator formulation. The method is briefly discussed here; the details can be found in the references.

The response is expanded in the form

$$\mathbf{x} = \sum_{m=1}^{\infty} [\zeta_m(t)\mathbf{y}_m + \eta_m(t)\mathbf{z}_m],$$

where $\zeta_m(t)$ and $\eta_m(t)$ are modal co-ordinates and $\mathbf{y}_m$ and $\mathbf{z}_m$ are the real and imaginary parts of the complex coupled eigenfunctions $\mathbf{h}_m$ of equation (28). Modal analysis yields

$$\dot{\zeta}_m - \omega_m \eta_m = F_m^z, \quad \dot{\eta}_m + \omega_m \zeta_m = F_m^y, \tag{43}$$

where $F_m^z = -\omega_m(\mathbf{z}_m, \mathbf{f})$, $F_m^y = \omega_m(\mathbf{y}_m, \mathbf{f})$ and $\mathbf{f}$ is the extended excitation vector [1]. Decoupling these equations and introducing small modal damping gives

$$\ddot{\zeta}_m + 2\rho_m\omega_m\dot{\zeta}_m + \omega_m^2\zeta_m = \dot{F}_m^z + \omega_m F_m^y, \tag{44}$$

$$\ddot{\eta}_m + 2\rho_m\omega_m\dot{\eta}_m + \omega_m^2\eta_m = \dot{F}_m^y - \omega_m F_m^z, \tag{45}$$

where ρ_m is the damping ratio for the mth mode.

6.1. SUPPORT MOTION EXCITATION

Consider the problem where the bearing support is subjected to a specified time-varying displacement. This case is of particular importance for systems such as disk drives. It also provides insight into the natural frequency veering phenomenon, the modal coupling between the disk and spindle, and the potential for energy transmission between components. The equations of motion are

$$\mathbf{M}\mathbf{h}_{tt} + \Omega\mathbf{G}\mathbf{h}_t + (\mathbf{L} - \Omega^2\tilde{\mathbf{L}})\mathbf{h} = \mathbf{0}, \tag{46}$$

with the time-varying boundary conditions

$$u|_{z=0} = f_1(t), \quad u_z|_{z=0} = 0, \quad v|_{z=0} = f_2(t), \quad v_z|_{z=0} = 0. \tag{47}$$

This problem with non-homogeneous boundary conditions is transformed into an equivalent forced vibration problem with homogeneous boundary conditions using the transformation

$$u(z, t) = \hat{u}(z, t) + f_1(t), \quad v(z, t) = \hat{v}(z, t) + f_2(t). \tag{48}$$

With the representation $\mathbf{h} = \hat{\mathbf{h}} + \tilde{\mathbf{h}}$ where $\mathbf{h} = [w\ u\ v\ u^c\ v^c\ \phi\ \psi]^T$, $\hat{\mathbf{h}} = [\hat{w}\ \hat{u}\ \hat{v}\ \hat{u}^c\ \hat{v}^c\ \hat{\phi}\ \hat{\psi}]^{\mathrm{T}}$ and $\tilde{\mathbf{h}} = [0\ f_1\ f_2\ f_1\ f_2\ 0\ 0]^T$, substitution into equation (46) gives

$$\mathbf{M}\hat{\mathbf{h}}_{tt} + \Omega\mathbf{G}\hat{\mathbf{h}}_t + (\mathbf{L} - \Omega^2\tilde{\mathbf{L}})\hat{\mathbf{h}} = \mathbf{f}, \tag{49}$$

where

$$\mathbf{f} = -\begin{pmatrix} 0 \\ \ddot{f}_1 - 2\Omega\dot{f}_2 - \Omega^2 f_1 \\ \ddot{f}_2 + 2\Omega\dot{f}_1 - \Omega^2 f_2 \\ \alpha(\ddot{f}_1 - 2\Omega\dot{f}_2 - \Omega^2 f_1) \\ \alpha(\ddot{f}_2 + 2\Omega\dot{f}_1 - \Omega^2 f_2) \\ 0 \\ 0 \end{pmatrix} \tag{50}$$

and components of $\hat{\mathbf{h}}$ satisfy homogeneous boundary conditions. $\tilde{\mathbf{h}}$ is known, so solution of equation (49) yields the complete solution $\mathbf{h}$.

Consider the base excitation where the bearing is subjected to a time-varying, vertical displacement $\sin pt$ in the ground-based (inertial) reference frame. Transforming this into rotating co-ordinates yields

$$u(0, t) = [\sin(p + \Omega)t + \sin(p - \Omega)t]/2, \quad v(0, t) = [\cos(p + \Omega)t - \cos(p - \Omega)t]/2,$$

and the forcing function (50) becomes

$$\mathbf{f} = \mathbf{f}_1 + \mathbf{f}_2 = p^2 \begin{pmatrix} 0 \\ \sin(p+\Omega)t \\ \cos(p+\Omega)t \\ \alpha\sin(p+\Omega)t \\ \alpha\cos(p+\Omega)t \\ 0 \\ 0 \end{pmatrix} + p^2 \begin{pmatrix} 0 \\ \sin(p-\Omega)t \\ -\cos(p-\Omega)t \\ \alpha\sin(p-\Omega)t \\ -\alpha\cos(p-\Omega)t \\ 0 \\ 0 \end{pmatrix}. \tag{51}$$

For each bearing excitation frequency p the effective force $\mathbf{f}$ and response $\hat{\mathbf{h}}$ are at two frequencies, $p \pm \Omega$. Consequently, resonant response occurs for $p = \omega \pm \Omega$, where ω are the natural frequencies of the coupled vibration modes (the uncoupled modes do not participate in the response). Figures 4(a, b), which are readily obtained from Figure 2, show the resonant excitation frequencies for the $\mathbf{f}_1$ and $\mathbf{f}_2$ components, respectively. Figures 5(a, b) show the response amplitudes of the disk at $r = 1$, $\theta = 0$ caused by the components $\mathbf{f}_1$ and $\mathbf{f}_2$ when Ω and p are varied. Notice that not all resonances predicted in Figure 4 appear in Figure 5. The qualitative explanation lies in the disk or spindle nature of the vibration modes [8]. Spindle modes are not prominent because the response is calculated on the disk, which is like a "node" for the spindle modes. Disk modes are not prominent because such modes are not excited by the purely spindle and clamp excitation (51). The disk response in Figure 5 is dominated by coupled modes that involve substantial disk *and* spindle deflection. The large peak in the response of the ω_7 mode in Figure 5(a) reflects this. Near the peak, ω_7 is veering away from ω_9 (Figure 2) and the vibration mode is changing rapidly from a disk mode to a spindle mode. The response is maximized in the veering zone where the mode is mixed and decays as the mode adopts disk ($\Omega < 4$) or spindle ($\Omega > 6$) character. Thus, bearing support motion may induce substantial vibration in the

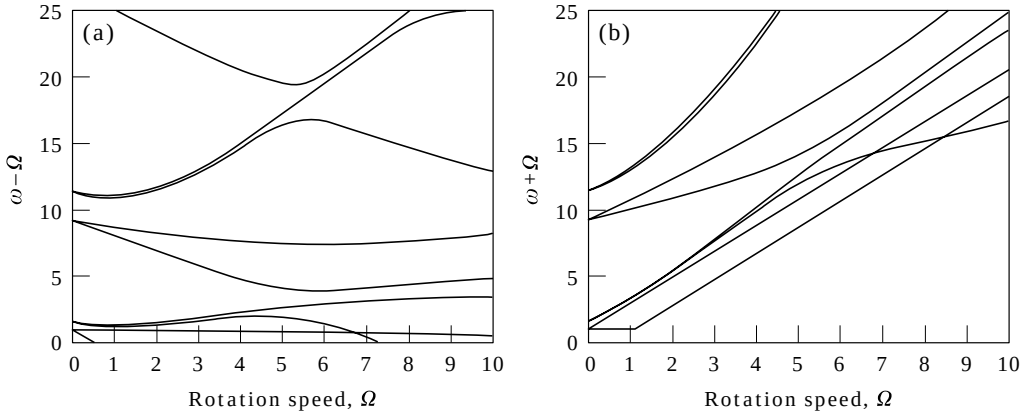

Figure 4. Variation of (a) $\omega - \Omega$ and (b) $\omega + \Omega$ with Ω, where ω is the natural frequency and Ω is the rotation speed.

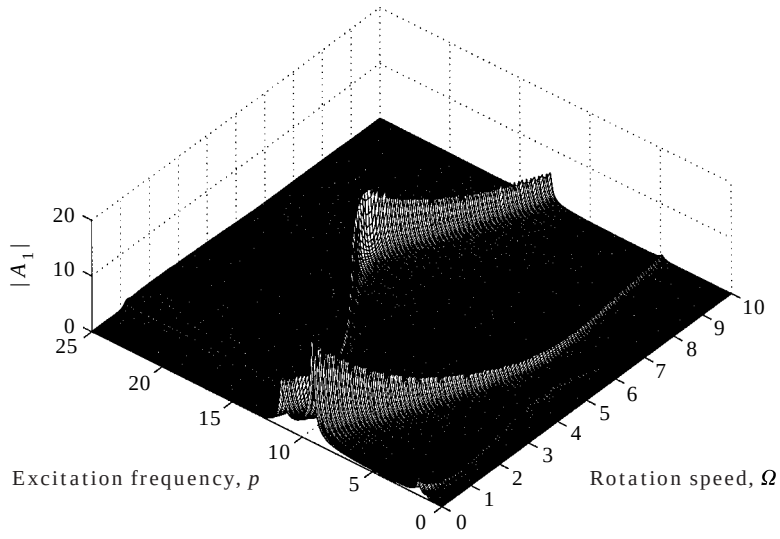

(a)

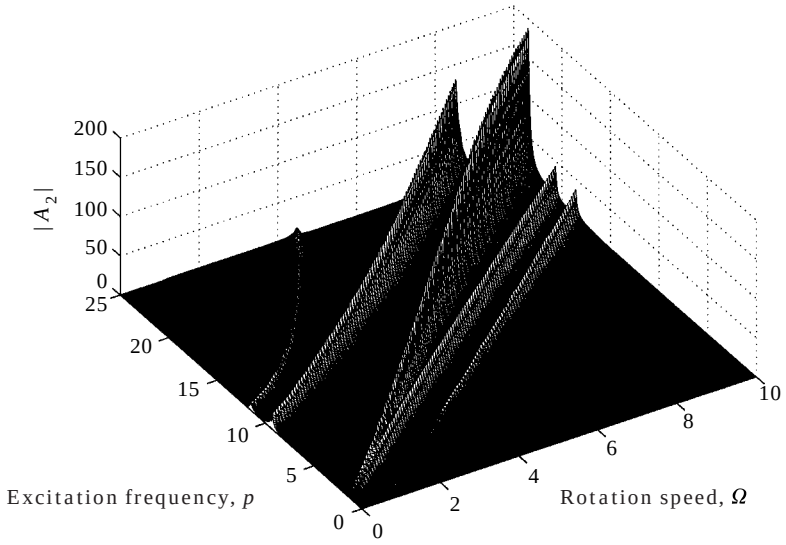

(b)

Figure 5. Transverse disk response amplitude at $r = 1$, $\theta = 0$ to the (a) $\mathbf{f}_1$ component of equation (51) and (b) $\mathbf{f}_2$ component of equation (51) for sinusoidal bearing excitation with frequency p.

disk in the absence of any other forcing. In general, spindle excitation can drive large disk response and *vice versa*, an important consideration in practical applications. Modes having mixed disk and spindle character are particularly susceptible to this transfer of energy.

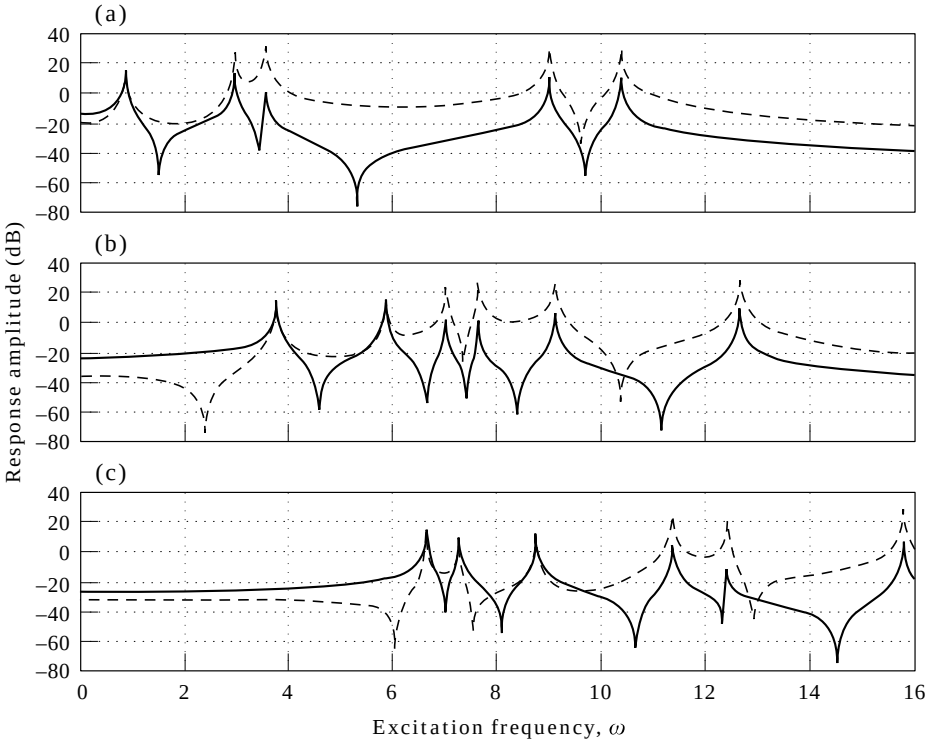

Figure 6. Frequency response at (a) $\Omega = 2$, (b) $\Omega = 5$ and (c) $\Omega = 8$. The excitation is $q_u(z, t) = \delta(z - 0{\cdot}7)e^{i\omega t}$. The solid lines denote the response on the spindle at $z = 0{\cdot}7$, that is $u(0{\cdot}7)$, and the dashed lines denote the response on the disk at $r = 1$, $\theta = 0$, that is $w(1, 0)$.

6.2. SPINDLE EXCITATION

As a second example, consider the case of direct spindle excitation where a sinusoidal point force in rotating co-ordinates acts along the direction of the deflection u at $z = 0{\cdot}7$, that is $q_u(z, t) = \delta(z - 0{\cdot}7)e^{i\omega t}$. Figure 6 shows the spindle and disk frequency response amplitudes at $\Omega = 2$, 5 and 8. This range encompasses the veering zone between the third and fifth modes as seen in Figure 2. Large, complementary changes in these vibration modes occur in the veering region: the third mode changes from a disk mode to a spindle mode and the fifth mode tends toward a disk mode from a spindle mode. The relative amplitudes of the resonant peaks demonstrate the change in character of the third and fifth modes. While the third mode peak is barely distinguishable in the spindle response at $\Omega = 2$, it is prominent at $\Omega = 8$. Correspondingly, the fifth mode peak is reduced as its character changes from disk to spindle mode. Both modes are prominent at $\Omega = 8$ where each mode has substantial disk and spindle deformation.

The foregoing forced response analyses were duplicated using a Galerkin discretization with the stationary system eigenfunctions as basis functions [1]. Six

pairs of stationary system eigenfunctions associated with the degenerate, coupled natural frequencies were used. The exact and Galerkin solutions show excellent agreement. Thus, as with the free vibration results of Figure 2, Galerkin discretization provides an accurate and efficient tool for response analyses.

7. SUMMARY AND CONCLUSIONS

1. A closed-form analytical solution to the eigenvalue problem of the rotating disk–spindle system is obtained. In conjunction with the extended operator formulation, the exact solution permits straightforward application of analytical procedures such as perturbation and modal analysis. The complex, speed-dependent eigenfunctions likely provide an excellent basis for discretization of disk–spindle systems in the presence of non-linear, time-varying, and dissipative effects.
2. The exact solution provides a valuable benchmark for evaluation of approximate methods. Galerkin discretization as presented in references [1, 8] provides excellent results for both eigensolutions and forced response. This approach is simpler to program and more computationally efficient than the exact solution.
3. For the parameter set considered, the convergence of the power series solution to the disk equation is markedly better for expansion about the ordinary point $r = 1$ than about the regular singular point $r = 0$. While the limited parameter range considered here does not permit general convergence conclusions, the large difference suggests superiority of the expansion about $r = 1$.
4. *Disk* critical speeds analogous to those of a rigidly supported spinning disk exist in addition to *spindle* critical speeds associated with vanishing eigenvalues. Furthermore, disk–spindle coupling introduces disk critical speeds associated with the one-nodal diameter coupled modes that do not exist for a rigidly supported disk. The critical speeds of a rigidly supported disk corresponding to the modes with numbers of nodal diameters other than one remain points of instability; these speeds are unaffected by disk–spindle coupling.
5. The extended operator formulation allows perturbation analysis of the zero speed and critical speed eigenvalue problems. This analysis yields simple formulae for the sensitivity of the zero speed natural frequencies and spindle critical speeds to changes in the non-dimensional parameters.
6. The analytical eigensolutions of the rotating disk–spindle system and the extended operator formulation admit a closed-form modal analysis for continuous gyroscopic systems to obtain the forced response. This technique is exploited to examine two cases, support motion and spindle excitation, that provide insight into the modal interaction associated with natural frequency veering and the transmission of excitation energy between the spindle and disk.

REFERENCES

1. R. G. PARKER 1999 *Journal of Applied Mechanics* **66,** 218–224. Analytical vibration of spinning, elastic disk–spindle systems.
2. G. T. FLOWERS and S. G. RYAN 1993 *Journal of Engineering for Gas Turbines and Power* **115**, 227–233. Development of a set of equations for incorporating disk flexibility effects in rotordynamic analyses.
3. J. A. DOPKIN and T. E. SHOUP 1974 *Journal of Engineering for Industry* **96**, 1328–1333. Rotor resonant speed reduction caused by flexibility of disks.
4. D. R. CHIVENS and H. D. NELSON 1975 *Journal of Engineering for Industry* **97**, 881–886. The natural frequencies and critical speeds of a rotating, flexible shaft-disk system.
5. N. KLOMPAS 1974 *ASME paper no*. 74-*GT*-159. Theory of rotor dynamics with coupling of disk and blade flexibility and support structure asymmetry.
6. F. S. WU and G. T. FLOWERS 1992 *Journal of Vibration and Acoustics* **114**, 242–248. A transfer matrix technique for evaluating the natural frequencies and critical speeds of a rotor with multiple flexible disks.
7. C.-W. LEE, H.-S. JIA, J.-H. SEO, C.-S. KIM and S.-B. CHUN 1997 *Proceedings of the ASME* 16*th Biennial Conference on Vibration and Noise*, *Paper DETC*97/*VIB*-4181. Prediction of coupled vibrations in hard disk drive spindle systems.
8. R. G. PARKER and P. J. SATHE (in press) *Journal of Vibration and Acoustics*. Free vibration and stability of a spinning disk–spindle system.
9. S. P. TIMOSHENKO and J. N. GOODIER 1970 *Theory of Elasticity*. New York: McGraw-Hill.
10. R. G. PARKER and C. D. MOTE JR. 1996 *Journal of Appled Mechanics* **63**, 953–961. Vibration and coupling phenomena in asymmetric disk–spindle systems.
11. C. M. BENDER and S. A. ORSZAG 1978 *Advanced Mathematical Methods for Scientists and Engineers*. New York: McGraw-Hill.
12. H. LAMB and R. V. SOUTHWELL 1921 *Proceedings of the Royal Society of London*, *A*, **99** 272–280. The vibrations of a spinning disk.
13. W. EVERSMAN and R. O. DODSON, JR. 1969 *AIAA Journal* **7**, 2010–2012. Free vibration of a centrally clamped spinning circular disk.
14. J. A. WICKERT and C. D. MOTE, JR. 1991 *Applied Mechanics Reviews* **44**, S279–S284. Response and discretization methods for axially moving materials.
15. R. G. PARKER 1999 *Journal of Sound and Vibration* **221**(2), 205–219. Supercritical speed stability of the trivial equilibrium of an axially moving string on an elastic foundation.
16. C. D. MOTE, JR. 1970 *Journal of the Franklin Institute* **290** 329–344. Stability of circular plates subjected to moving loads.
17. A. A. RENSHAW and C. D. MOTE, JR. 1992 *Journal of Applied Mechanics* **59**, 687. Absence of one nodal diameter critical speed modes in an axisymmetric rotating disk.
18. L. MEIROVITCH 1975 *Journal of Applied Mechanics* **42** 446–450. A modal analysis for the response of linear gyroscopic systems.
19. G. M. T. D'ELEUTERIO and P. C. HUGHES 1984 *Journal of Applied Mechanics* **51**, 415–422. Dynamics of gyroelastic continua.